CONDENSED MATTER PHYSICS

Topological magnon insulators in two-dimensional van der Waals ferromagnets $CrSiTe_3$ and $CrGeTe_3$: Toward intrinsic gap-tunability

Fengfeng Zhu[1,2]*†, Lichuan Zhang[3,4†], Xiao Wang[1†], Flaviano José dos Santos[3,5], Junda Song[1], Thomas Mueller[1], Karin Schmalzl[6], Wolfgang F. Schmidt[6], Alexandre Ivanov[7], Jitae T. Park[8], Jianhui Xu[8,9], Jie Ma[2], Samir Lounis[3,10], Stefan Blügel[3], Yuriy Mokrousov[3,11]*, Yixi Su[1]*, Thomas Brückel[12]

The bosonic analogs of topological insulators have been proposed in numerous theoretical works, but their experimental realization is still very rare, especially for spin systems. Recently, two-dimensional (2D) honeycomb van der Waals ferromagnets have emerged as a new platform for topological spin excitations. Here, via a comprehensive inelastic neutron scattering study and theoretical analysis of the spin-wave excitations, we report the realization of topological magnon insulators in $CrXTe_3$ (X = Si, Ge) compounds. The nontrivial nature and intrinsic tunability of the gap opening at the magnon band-crossing Dirac points are confirmed, while the emergence of the corresponding in-gap topological edge states is demonstrated theoretically. The realization of topological magnon insulators with intrinsic gap-unability in this class of remarkable 2D materials will undoubtedly lead to new and fascinating technological applications in the domain of magnonics and topological spintronics.

INTRODUCTION

Recent theoretical predictions and experimental realizations of exotic quasiparticles and topological excitations in condensed matter have led to a tremendous research interest in topological quantum materials (*1*–*5*). The topology of the electronic band structure is closely linked to the Berry curvature in the *k*-space (*6*, *7*), for which the spin-orbit coupling (SOC) plays a key role. In principle, it is also possible to realize nontrivial topology in a bosonic system, such as a system of magnonic excitations (*8*–*18*), since the band topology can be treated independently from the statistical nature of the particles. Such topological excitations and the corresponding nontrivial in-gap edge states are chiral and robust against disorder; it is thus believed that the emergence and manipulation of the topological magnonic states bare a tremendous promise for future applications in magnonics and topological spintronics, such as, e.g., quantized pumping of magnons (*19*), spin-wave beam splitter (*10*), magnon waveguides (*20*), chiral traveling-wave magnon amplifiers (*21*), and magnon-driven orbitronics (*22*).

However, in contrast to the case of fermionic systems, the topological excitations have been realized only in very few bosonic systems. This is largely owing to the lack of suitable candidate materials as well as to the tremendous challenges in experimental probes of uncharged bosonic topological excitations and, in particular, in a direct detection of in-gap surface/edge states. For instance, inelastic neutron scattering may be the method of choice, e.g., for disentangling topological excitation gaps, but, to directly probe the in-gap edge excitation mode is unfortunately beyond its reach even with the most powerful neutron instruments available nowadays. Nevertheless, since topological magnon edge states contribute to the transverse thermal Hall conductivity, it has recently been demonstrated that the nontrivial topological nature of the magnonic bands can be manifested experimentally by the thermal Hall effect even in a charge-neutral spin system (*23*–*26*).

Following the pioneering study of the magnon thermal Hall effect in the pyrochlore ferromagnet $Lu_2V_2O_7$ (*23*, *24*), the evidence for the gapped magnonic topological insulating phase was reported in the Ising-like kagome ferromagnet Cu[1,3-bdc] under applied magnetic field via inelastic neutron scattering (*8*). The search for topological excitations in various spin systems has been intensified since then. Recently, Dirac magnons that exhibit symmetry-protected band crossings have been observed in a three-dimensional (3D) Heisenberg antiferromagnet Cu_3TeO_6 (*15*, *16*) and in a 3D quantum *XY* magnet $CoTiO_3$ (*17*). Meanwhile, 2D honeycomb van der Waals (vdW) magnets (*27*–*29*), such as the 2D ferromagnets $CrGeTe_3$ and Fe_3GeTe_2 as well as the Kitaev material α-$RuCl_3$, have attracted tremendous research interest owing to their fascinating physical properties. Since the recent observation of the gapped topological excitations in ferromagnetic CrI_3 (*11*), 2D vdW honeycomb-lattice magnets start to emerge as a unique platform for the exploration of the topological magnonics (*9*, *12*, *14*). In this class of materials, as schematically shown in Fig. 1A, a topological gap can be opened at the magnon band-crossing Dirac points when a sufficiently large SOC is present. Pronounced SOC would, in turn, give rise to antisymmetric or anisotropic exchange interactions, such as the

[1]Jülich Centre for Neutron Science (JCNS) at Heinz Maier-Leibnitz Zentrum (MLZ), Forschungszentrum Jülich, Lichtenbergstrasse 1, D-85747 Garching, Germany. [2]Department of Physics and Astronomy, Shanghai Jiao Tong University, 200240 Shanghai, China. [3]Peter Grünberg Institut and Institute for Advanced Simulation, Forschungszentrum Jülich and JARA, 52425 Jülich, Germany. [4]Department of Physics, RWTH Aachen University, 52056 Aachen, Germany. [5]Theory and Simulation of Materials (THEOS), and National Centre for Computational Design and Discovery of Novel Materials (MARVEL), École Polytechnique Fédérale de Lausanne, 1015 Lausanne, Switzerland. [6]Jülich Centre for Neutron Science (JCNS) at ILL, Forschungszentrum Jülich, F-38000 Grenoble, France. [7]Institut Laue-Langevin, 71 Avenue des Martyrs CS 20156, 38042 Grenoble Cedex 9, France. [8]Heinz Maier-Leibnitz Zentrum (MLZ), Technische Universität München, D-85747 Garching, Germany. [9]Helmholtz-Zentrum Berlin für Materialien und Energie GmbH, Hahn-Meitner-Platz 1, D-14109 Berlin, Germany. [10]Faculty of Physics, University of Duisburg-Essen and CENIDE, 47053 Duisburg, Germany. [11]Institute of Physics, Johannes Gutenberg University Mainz, 55099 Mainz, Germany. [12]Jülich Centre for Neutron Science JCNS and Peter Grünberg Institut PGI, JARA-FIT, Forschungszentrum Jülich, D-52425 Jülich, Germany.
*Corresponding author. Email: f.zhu@fz-juelich.de (F.Z.); y.mokrousov@fz-juelich.de (Y.M.); y.su@fz-juelich.de (Y.S.)
†These authors contributed equally to this work.

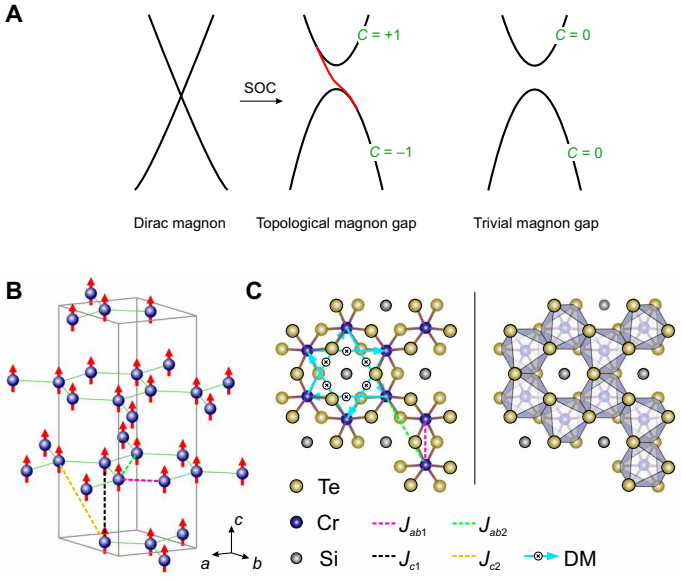

Fig. 1. Schematic of the trivial and topological magnon bands and of the magnetic and atomic structures of $CrXTe_3$. (**A**) Schematic of the band dispersion for a Dirac magnon, a topological magnon, and a trivial magnon. (**B**) Magnetic structure of $CrSiTe_3$. In the *ab* plane, the Cr atoms form a honeycomb lattice represented by the dark blue spheres and green solid lines. The magnetic moments are represented by red arrows. The first and second NN exchange interactions in intra- and inter-planes are represented by purple, green, black, and yellow dashed lines, respectively. (**C**) View perpendicular to the *ab* plane showing the honeycomb network of $CrSiTe_3$. The honeycomb network is caged by the edge-sharing octahedra composed of Te atoms and Si—Si dimers located at the center. The light blue arrows represent the bond directions of the DM interactions between the second NN Cr atoms, and all the DM vectors share a common sign along the *c* axis.

Dzyaloshinskii-Moriya (DM) (*30*) and Kitaev interactions, which can drive nontrivial magnonic topology.

While the current research focus of the community falls primarily on few-layer vdW heterostructures and Morié superlattices, a variety of recently found quantum phenomena in bulk vdW materials—e.g., the half-integer thermal quantum Hall effect and fractionalized Majorana fermions in α-$RuCl_3$ (*29*) or topological magnetic textures in Fe_3GeTe_2 (*28*)—clearly indicate the potential of bulk, quasi-2D vdW magnetic materials as a rich playground in topological quantum matter research. A thorough understanding of intrinsic magnetic interactions and emergent topological properties in single-crystal bulk samples will undoubtedly stimulate further research on monolayer, few-layer, and Morié-based counterparts. In this context, 2D vdW $CrXTe_3$ compounds emerge as one of the very promising representatives in this class. One would expect the existence of topological magnons in $CrXTe_3$ similarly to CrI_3 (*9*, *18*, *26*), as long as SOC and the antisymmetric exchange interactions are strong enough in this ferromagnetic honeycomb system. Furthermore, because of high versatility in terms of chemical composition, a range of topological magnon insulators with intrinsic gap-tunability may be realized in the $CrXTe_3$ family. Hence, the intrinsic control of topological magnon properties, for instance, via the engineering of DM interaction, may lead to novel applications in magnonic spintronics and quantum technology.

In this work, we present a comprehensive inelastic neutron scattering study of the spin-wave excitations in single-crystal $CrSiTe_3$ and $CrGeTe_3$, which belong to a family of 2D vdW honeycomb ferromagnets. Our inelastic neutron scattering experiments performed at low temperatures show clear dispersive magnonic bands and a well-resolved bandgap opening at the high-symmetry *K* points in the Brillouin zone (BZ). By fitting to experimental data within the linear spin wave theory (LSWT), the magnitude of exchange interactions in studied materials has been determined. Moreover, the observed bandgap opening was ascribed to the antisymmetric exchange interactions, namely, the DM interaction, and a spin Hamiltonian model including the second nearest-neighbor (2nd-NN) DM interaction could provide a very good description of the magnonic dispersion in $CrXTe_3$. In line with expectations, the size of the topological gap was found to be strongly dependent on the strength of the DM interaction that intrinsically originates from SOC in this system. Furthermore, the Chern numbers of the magnonic bands were found to be nonzero, thus indicating that the bandgap opening is indeed topologically nontrivial and corresponding edge states could emerge inside the gap. By theoretically assessing the magnitude of the thermal Hall effect, we find that the topologically nontrivial features could be detected in thermal transport measurements in two considered systems. On the basis of the compelling evidence obtained in our inelastic neutron scattering experiments and theoretical calculations, we thus conclude that the exotic topological magnon insulator, which is intrinsically gap tunable, can be ideally realized in the family of 2D vdW honeycomb ferromagnets $CrXTe_3$.

RESULTS AND DISCUSSION

High-quality single crystals of $CrXTe_3$ (X = Si, Ge) were grown by the flux method and were carefully examined by x-ray Laue, single-crystal x-ray, and neutron diffraction. The Cr^{3+} ions with $S = 3/2$ in $CrXTe_3$ (X = Si, Ge) occupy an *ABC* stacked honeycomb lattice, as shown in Fig. 1B. Despite the presence of the Si/Ge atoms, each layer shares a similar atomic structure to that of the chromium trihalides CrI_3 (*31*) and $CrBr_3$ at low temperature. All the Cr^{3+} ions are located in the center of the edge-shared trigonal distorted octahedra (D_{3d} symmetry) composed of Te atoms, as shown in Fig. 1C. Below T_c, both materials exhibit ferromagnetic order with the magnetic moments aligned along the *c* axis. As shown in fig. S1, the magnetic susceptibilities measured with fields applied along the *a* and *c* axes clearly show ferromagnetic phase transitions occurring at ~33 and ~63 K for $CrSiTe_3$ and $CrGeTe_3$, respectively, with the easy axis along the *c* axis. As the isothermal magnetization curves shown in fig. S1, their magnetic moments can be easily aligned and saturated along both the *a* and *c* axes by an application of a small magnetic field, which indicates a small magnetic anisotropy energy in these two materials, consistent with the previous magnetization measurements (*32*–*35*). In addition, the ferromagnetic transitions are further confirmed by neutron diffraction, and the transition temperatures T_c are extracted from the fitting of the temperature-dependent intensity of the (1,1,0) magnetic Bragg peak. Among them, the magnetic moment direction of $CrGeTe_3$ in the ferromagnetic phase is determined along the *c* axis by polarized neutron diffraction, as shown in fig. S2.

In Fig. 2, we show the magnon spectra of $CrSiTe_3$ along the high-symmetry directions [−1,H,0] and [H,H,3] in the (H,K,0) reciprocal plane as well as along the [1,1,L] direction in the (H,H,L) reciprocal plane. The measured momentum transfer *Q* positions in reciprocal space are shown as the black solid lines in the inset of

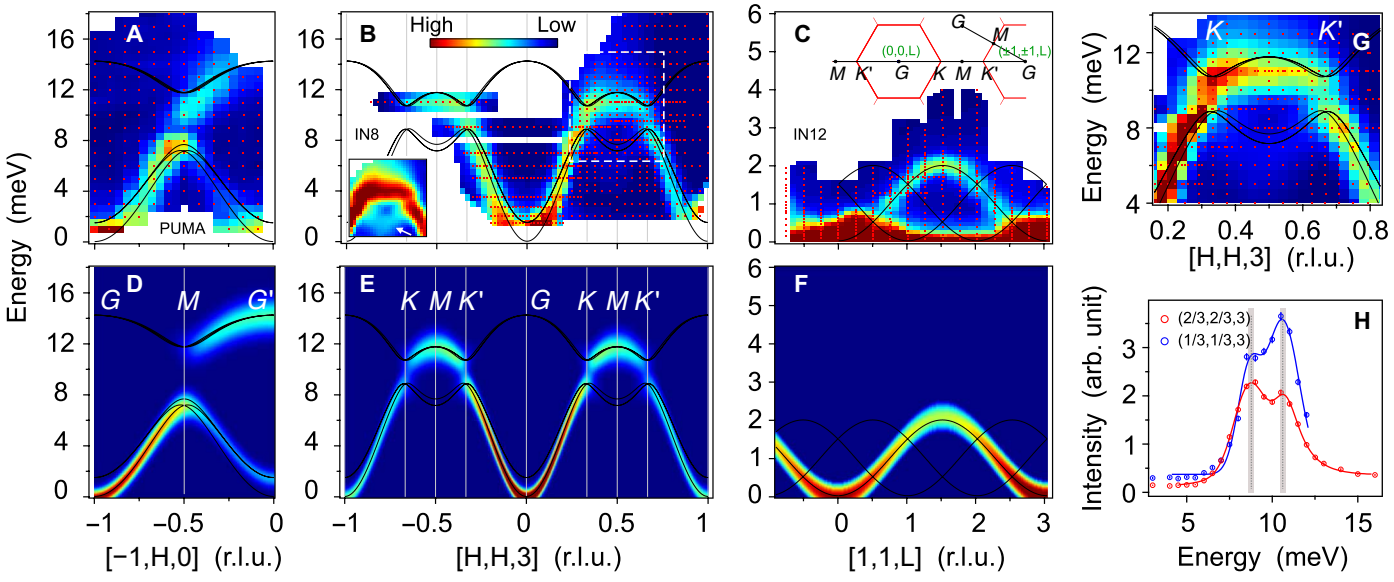

Fig. 2. Spin-wave excitations in $CrSiTe_3$. (**A** to **C**) Energy- and momentum-resolved neutron scattering intensity maps of magnons in $CrSiTe_3$ along the high-symmetry directions measured at the thermal neutron triple-axis spectrometer PUMA and IN8 and at the cold neutron triple-axis spectrometer IN12, respectively. The black solid lines are the calculated magnon dispersion curves based on the parameters of Heisenberg-DM model presented in this paper. The inset in (B) is a contrast-adjusted plot for the dashed rectangle part to make the acoustic branch easy to see. The inset in (C) shows the exact scan paths in the reciprocal space. (**D** to **F**) Calculated magnon spectra intensity maps for (A) to (C), respectively. The calculated spectra are convolved with an energy resolution of 1 meV to compare with the experimental data. (**G**) Zoom-in plot of the magnon spectra from (B) near the *K* points. (**H**) Energy scans of magnon density of states at the *K* points. The solid lines are the two-peak Gauss fitting results, and the fitted peak positions and error bars are indicated by the vertical dashed lines with gray shadow. r.l.u, reciprocal lattice unit.

Fig. 2C. The measured magnon bands lie below 16 meV and show clear dispersion along all directions. As shown in Fig. 2A, the low-energy magnon mode (referred to as "acoustic" magnon mode) emerges from the BZ center Γ point and reaches its maximum energy with a gap opening at the *M* point of the in-plane BZ boundary, consistently with its ferromagnetic nature. Along the [H,H,3] direction, in the vicinity of the *K* points, as shown in Fig. 2B, a small spin gap is faintly visible at $E \approx 9$ meV. Besides, as highlighted by the white arrow in the inset of Fig. 2B, a new branch connected to the acoustic magnon mode was observed along the BZ boundary *K*-*M*-*K*′ direction although its intensity is rather weak. From a zoom-in plot in Fig. 2G, the high-energy branch (referred to as "optical" magnon mode) is found to be less dispersive as compared to the acoustic magnon mode, and it also seems disconnected from the acoustic branch at *K* points. To further confirm whether a magnon gap is opened at the *K* point, the line profiles of the constant-Q scans at two different *K* points are shown in Fig. 2H, where a gap opening of about 2 meV can be clearly resolved. Subsequently, the maximum of the acoustic and the minimum of the optical magnon mode at the *K* point are determined as 8.6(1) meV and 10.7(1) meV by the multipeak fitting, respectively. Given that the magnitude of the gap is quite large and no clear phonon modes are observed, we conclude that the magnon-phonon hybridization is unlikely to be the origin of the observed gap opening. Instead, introducing an antisymmetric exchange interaction, such as the DM interaction, into the spin Hamiltonian could potentially induce such a considerable gap at the *K* point. As for the [1,1,L] direction, the acoustic magnon mode only extends up to 2 meV, which is much smaller than that in the Γ-*M* and Γ-*K* directions, indicating that the coupling between vdW layers is notably weak and that the magnon spectra are mainly dictated by the intralayer exchange interactions.

As for the analogous $CrGeTe_3$, whose transition temperature T_c is nearly doubled as compared to that of $CrSiTe_3$, we also measured its spin waves along all high-symmetry directions, and the black solid lines in the inset of Fig. 3B show the corresponding *Q* positions for the measurements. The magnon modes in the (H,K,0) reciprocal plane are shown in Fig. 3A, where two branches, namely, the acoustic and optical modes, can be easily distinguished, and the magnon modes along [1,1,L] directions, dictated by the interlayer exchange interactions, are shown in Fig. 3B. As expected, the acoustic mode has a stronger dispersion than the optical mode and also emerges from the magnetic BZ center Γ point at low energy. Except for the scale of the energy transfers, the overall feature of the magnon modes of $CrGeTe_3$ appears very similar to that of $CrSiTe_3$ including the gap opening at the *K* point. The acoustic magnon mode in the (H,K,0) plane reaches its energy maximum at around 15 meV, which is nearly two times that of $CrSiTe_3$, but, along the out-of-plane direction, the magnon mode only extends to 2.5 meV, basically the same as in $CrSiTe_3$. It indicates that replacing the Si atoms by heavier Ge atoms in $CrXTe_3$ will notably enhance the intralayer exchange interactions and, meanwhile, will have little influence on the interlayer exchange interactions. This suggests that the exchange interactions can be tuned by nonmagnetic atoms without destroying the magnetic network and that the strength of SOC of nonmagnetic atoms may also play an important role in the superexchange interactions in this vdW honeycomb ferromagnet family.

Furthermore, one can notice that the optical mode of $CrGeTe_3$ is rather broad in energy even after taking into consideration the instrument resolution of ~2 meV at such energy transfer, and is quite intense, in contrast to the situation of $CrSiTe_3$. We find that the intensity of this optical magnon branch at the *K* point is about four times higher than the prediction of our LSWT calculation.

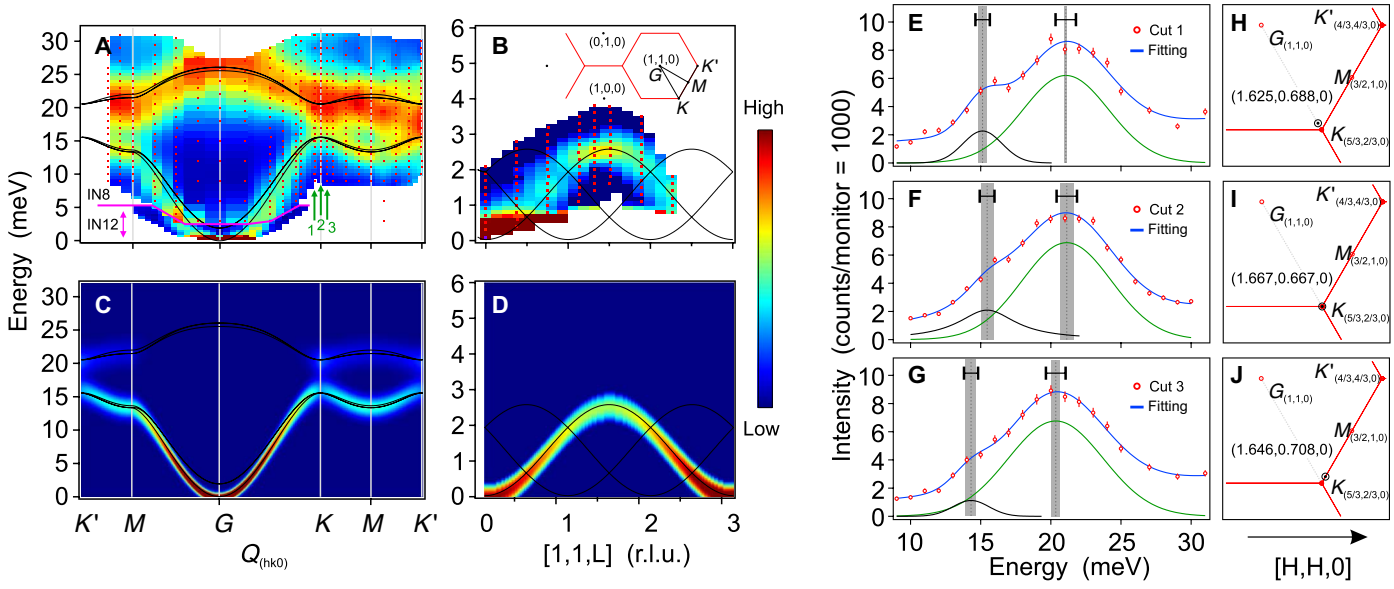

Fig. 3. Spin-wave excitations in $CrGeTe_3$. (**A** and **B**) Energy- and momentum-resolved neutron scattering intensity maps of magnon in $CrGeTe_3$ along the high-symmetry directions measured at IN8 and IN12, respectively. Black solid lines are the calculated magnon dispersion curves. Inset in (B) shows the projected BZ with high-symmetry points and the scan paths in the experiments. (**C** and **D**) The corresponding calculated magnon spectra intensity maps for (A) and (B) by using the 2nd-NN DM interaction model. The calculated spectra are convolved with an energy resolution of 1 meV to compare with experimental data. (**E** to **G**) The line profiles of constant-Q energy scan at the positions of 1,2,3 marked by the green arrows in (A) near the *K* point *Q* = (5/3,2/3,0). The solid lines are the multipeak Gauss fitting results. The peak positions and the errors are indicated, respectively, by the dashed lines and the gray shadows; the corresponding energy resolutions are represented by the black horizontal bar with caps. (**H** to **J**) The actual *Q* positions of the cut 1, 2, and 3 are marked by black circles with center dots in the reciprocal space. The red solid lines are the BZ boundaries.

Given that the optical phonon mode of $CrGeTe_3$ has a similar energy scale (*36*) and that the evidence for the spin-lattice coupling in $CrGeTe_3$ has already been reported in previous Raman experiments (*37*, *38*), we tend to believe that both the broadening in energy and the intensity enhancement could be a result of possible magnon-phonon interactions. The phonon modes around 25 meV are indeed mainly contributed by the magnetic atoms Cr (*39*); the coexistence of the phonon and magnon modes in the same energy range may allow for a possible spectral weight transfer between them, thus leading to the observed unusual intensity enhancement. Generally, a dynamic spin-lattice coupling can create hybridization gaps or broadening in the magnon spectra at the intersection points of the coupled magnon and phonon modes.

Regardless of the unusual broadening of the optical branches, a gap opening at the *K* point is still resolvable. In Fig. 3 (E to G), three line profiles of energy scans are extracted from the vicinity of the *K* point and fitted by two Gauss peaks to accurately determine the size of the opened gap, and the corresponding positions of momentum transfer in reciprocal space in the measurements are marked by the black circles in Fig. 3 (H to J). From Fig. 3F, a weak but clear shoulder can be seen around 15 meV, which denotes the band maximum of the acoustic mode, and subsequently, the size of the opened gap at the *K* point can be determined as ~5 meV from the fitting results. We conclude that such a large gap is unlikely to arise as a result of possible magnon-phonon coupling, since the magnon-phonon coupling–induced gap always occurs at the intersection between the magnon and phonon bands and it does not extend over the entire BZ. It is thus expected that the gap in $CrGeTe_3$ shares the same origin as in $CrSiTe_3$, namely, the antisymmetric exchange interaction, e.g., similar to the SOC-mediated DM interaction. Hence, it appears natural that a larger gap opening in $CrGeTe_3$ must arise from the larger SOC in the latter material when Si is replaced by heavier Ge.

To determine the nature of magnon bands and the underlying magnetic exchange interactions in $CrXTe_3$ systems, we carry out LSWT calculations based on a generalized Heisenberg spin Hamiltonian including DM interaction and single-ion magnetic anisotropy (*40*)

$$H = -\sum_{i<j} J_{ij}(\mathbf{S}_i \cdot \mathbf{S}_j) - A_{zz}\sum_i (S_i^z)^2 - \sum_{i<j} \mathbf{D}_{ij} \cdot (\mathbf{S}_i \times \mathbf{S}_j) \quad (1)$$

where J_{ij} is the Heisenberg exchange constant between spins $\mathbf{S}_i$ and $\mathbf{S}_j$, $\mathbf{D}_{ij}$ represents the vector of the DM interaction between two magnetic ions when the inversion symmetry is broken, and A_{zz} is the easy-axis anisotropy along the *c* axis. Note that we take $S = 3/2$ given that the measured moment of Cr ions is extracted as ~3 μ_B from the isotherm magnetization curve shown in fig. S1. As illustrated in Fig. 1B, we consider the 1st- and 2nd-NN Heisenberg exchange couplings in every honeycomb plane labeled as J_{ab1} and J_{ab2}, and the 1st- and 2nd-NN exchange couplings between layers labeled as J_{c1} and J_{c2}. From the symmetry analysis, there will be no DM interaction between the nearest neighbors (NNs) because of the space inversion. However, the space inversion symmetry is broken between the second NNs, which can lead to a nonzero 2nd-NN DM interaction.

After a proper fitting process of the experimentally observed magnon spectra along the high-symmetry directions, the best-fit values for the exchange parameters of $CrSiTe_3$ and $CrGeTe_3$ were extracted. As shown in Table 1, we find that the intralayer interactions

in $CrXTe_3$ are mainly dominated by the NN exchange couplings J_{ab1}, which are one order of magnitude larger than the interlayer exchange. Given the presence of sizeable interlayer exchange interactions, it is worth noting that $CrXTe_3$, strictly speaking, should be classified as quasi-2D spin systems. While the direct exchange coupling between Cr ions is expected to be antiferromagnetic due to the formation of Cr—Te—Cr bonds with a bond angle of nearly 90°, the NN exchange couplings among Cr ions become ferromagnetic ($J > 0$) according to the Goodenough-Kanamori-Anderson rules (*41*). Although the fitting values of the interlayer couplings J_{c1} and J_{c2} are quite comparable, the magnon dispersion along the [0,0,L] direction is likely much more sensitive to the 2nd-NN interlayer coupling J_{c2} because each Cr^{3+} spin has nine 2nd-NNs but only one 1st-NN. Besides, the strength of the DM interactions is fitted as $|\mathbf{D}_{ij}| = 0.12$ meV for $CrSiTe_3$ and $|\mathbf{D}_{ij}| = 0.32$ meV for $CrGeTe_3$, which results in a ~2- and ~5-meV gap opening at the *K* points, respectively. We remark that the magnitude of the DM interaction in $CrXTe_3$ constitutes about 10% of J_{ab1}, and it is quite comparable to the value of exchange J_{ab2} between 2nd-NN Cr ions. From the isothermal magnetization curve at 2 K (fig. S1), we can extract the magnetocrystalline anisotropy energy per Cr^{3+}, which is only 0.09 meV for $CrSiTe_3$ and 0.02 meV for $CrGeTe_3$, indicating a small single-ion anisotropy in the $CrXTe_3$ system. In terms of the small single-ion anisotropy, as expected, we failed to determine the size of the gap at the Γ point from our energy scan data directly, and we used instead the quadratic fitting result 0.01 meV (shown in figs. S5 and S6) for the anisotropy term *A* in the Heisenberg-DM model.

As shown in Fig. 2 (D to F) and Fig. 3 (C and D), the magnon bands of $CrXTe_3$ calculated from the Heisenberg-DM model are consistent with our experimentally observed spectra, taking into account a finite energy resolution. Especially in the vicinity of the *K* points, the opened gap is also well described by the model. In addition, a range of constant energy slices near the BZ boundary are found to be in an excellent agreement with the simulation results, as shown in fig. S4. Moreover, the calculated spectra also reproduce the characteristic weak/strong intensity of the magnon bands in different BZs, except that the optical modes of $CrGeTe_3$ are notably enhanced by the possible hybridization with the phonon modes, as discussed above.

The overall band dispersion is mainly determined by the ferromagnetic NN Heisenberg exchange couplings, and the gap opening at the *K* points cannot be reproduced by simply adding exchange couplings with further neighbors in the model, until an anisotropic exchange coupling term such as the DM interaction is taken into consideration. It is known that the DM interaction acts as an effective gauge potential for magnonic states and it can open topologically nontrivial bandgaps in a magnonic system (*9*, *42*). Without the DM interaction, a crossing point located in the vicinity of *K* point would be present (Fig. 4A), while the gap is opened immediately as the DM interaction is introduced, with the bandgap size increasing almost linearly with the strength of the DM interaction (Fig. 4B). Overall, the constructed Heisenberg-DM model reproduces spin waves in $CrXTe_3$ very nicely, with one key point being that the DM interaction in our case is not only dependent on the SOC strength of Te atoms along the Cr—Te—Cr paths but also influenced by Si/Ge atoms. The large difference of the gap size in $CrXTe_3$ thus translates into a possibility to tune the DM interaction by the substitution of the atoms with different SOC strength in the honeycomb center.

In addition to the Heisenberg-DM model, introducing the Kitaev interactions can also produce similar spin-wave spectra and induce a gap opening at the *K* points. If we exclude X atoms, the rest of $CrXTe_3$ shares a common atomic structure with the well-studied Kitaev spin liquid candidate α-$RuCl_3$ (*43*), and three kinds of diamond-shaped planes, composed of the NN Cr—Te—Cr bonds, are nearly orthogonal to each other. In terms of the structure symmetry, it is possible to have an anisotropic exchange interaction between NN, for instance, an anisotropic Ising interaction in the local basis that consists of the

Table 1. Spin Hamiltonian parameters. The values of exchange interactions including the DM interactions are listed together for both $CrSiTe_3$ and $CrGeTe_3$. The value of the 2nd-NN DM vector was chosen to reproduce the experimental spin-wave dispersion. The unit of the parameters indicated here is milli–electron volts. The single-ion anisotropy is fixed to 0.01 meV.

Unit (meV)	J_{ab1}	J_{ab2}	J_{c1}	J_{c2}	$\mathbf{D}_{ij}$
$CrSiTe_3$	1.49	0.15	0.07	0.06	(0,0,0.12)
$CrGeTe_3$	2.73	0.33	0.10	0.08	(0,0,0.32)

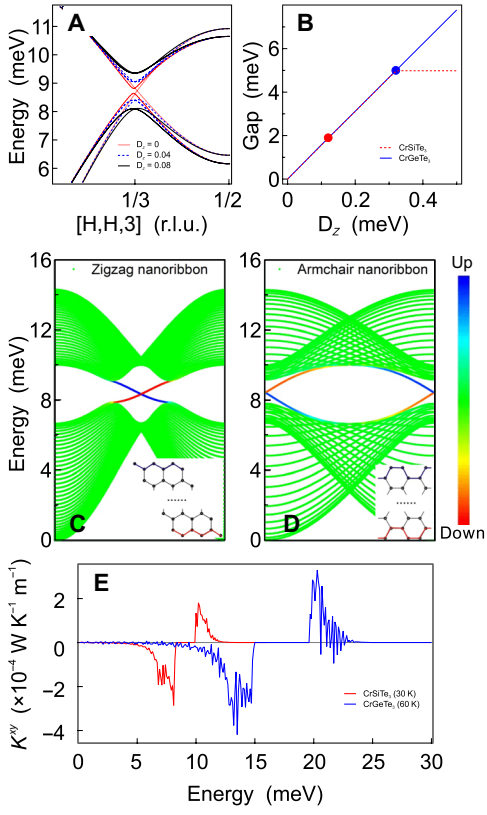

Fig. 4. The impact of the DM interaction on the magnon dispersion. The magnon dispersions of $CrSiTe_3$ with different DM interaction strength are compared in (**A**). (**B**) The relationships between the opened global bandgap and the strength of the DM interaction; the red and blue filled circles correspond to the values extracted from the magnon bands. (**C** and **D**) The edge states of the monolayer $CrSiTe_3$ for the respective zigzag and armchair nanoribbon. The color scale represents the weight of the magnonic wave function along the slab. (**E**) Temperature dependence of the topological thermal Hall conductivity of $CrSiTe_3$ and of $CrGeTe_3$ in the ferromagnetic ordered phases.

normal vectors of three Cr—Te—Cr planes, as shown in fig. S7. The presence of the additional anisotropy can make it possible to construct the Heisenberg-Kitaev Hamiltonian. Unexpectedly, to match the magnetic excitations in $CrXTe_3$, we found that the Kitaev exchange needs to be one order of magnitude larger than the NN Heisenberg term, as shown in table S1. In the latter case, the fitted Kitaev exchange parameters of $CrGeTe_3$ are almost two times those of $CrSiTe_3$, which is quite interesting, since $CrSiTe_3$ and $CrGeTe_3$ share a similar local environment including the bond distance for NN Cr atoms. One possible explanation would be that the *sp*3 hybridized orbitals of Si/Ge atoms in the honeycomb center are strongly coupled with the *p* orbitals of Te atoms and subsequently strongly influence the strength of the Cr—Te—Cr superexchange interaction. Similar orbital hybridization effect is not rare since the superexchange interaction mediated by nonmagnetic ions is also proposed in inverse-trirutile compound (*44*) and double perovskites (*45*). In any case, if $CrXTe_3$ is dominated by the Kitaev interaction, then a strong in-plane anisotropy should be easily evident in the magnetization measurements, which has never been reported. We thus conclude that the Heisenberg-Kitaev model is not a proper model for $CrXTe_3$. More details concerning the discussion of Heisenberg-Kitaev model are given in the Supplementary Materials.

Having determined the microscopic spin Hamiltonians for $CrXTe_3$, we turn to the analysis of the topological nature of the magnonic bands and reveal theoretically the presence of a large thermal Hall effect, an unambiguous experimental signature of topologically nontrivial in-gap edge states. Our numerical calculations confirm a nonzero Berry curvature at the *K* points and also a nonzero Chern number, indicating nontrivial topology of these magnon bands. For bulk $CrXTe_3$, the total Chern number is determined to be −3 and +3 for the acoustic and optical magnon bands, respectively, which means that there is one topological edge state at the boundary of each honeycomb layer. The sign of the Chern number depends on the magnetization direction, which, in our case, is the *z* axis. The sign of the Chern number can be changed by reversing the magnetization direction, which can be naturally achieved at the magnetic domain walls in $CrXTe_3$, acting as perfect waveguides for the topological edge states. In addition to the bulk system, we also investigated the topological properties of the monolayer system, where we observe an almost identical BZ Berry curvature distribution and predict only one acoustic branch with Chern number −1 and one optical branch with Chern number +1 for the magnon bands. Because of the lack of any interlayer interactions, the magnon bands in the monolayer are not split as in the bulk, but the topological properties are sustained as long as the intralayer DM interaction exists. To simplify the calculation, we use the monolayer system to study the edge states. The edge states of zigzag and armchair nanoribbons with the projections of the bulk states are shown together in Fig. 4 (C and D), where one can observe that the edges on the two sides of a nanoribbon hold their own exclusive edge states but with opposite propagation direction. The role of the DM interaction here is similar to that of strong SOC in graphene-like systems that turns them into a quantum spin Hall insulator (*2*), and so, $CrXTe_3$ can also be considered as a bosonic version of the well-known topological insulator state. Correspondingly, the presence of nontrivial edge states can contribute to the transverse thermal Hall conductivity to yield the topological thermal Hall effect when a longitudinal temperature gradient and out-of-plane magnetic field are applied. As shown in Fig. 4E, our numerical estimates indicate that the thermal Hall conductivity generated by the edge states can reach the order of 10^{-4} W $K^{-1}m^{-1}$, which is large enough to be observed in experiment. This motivates the future confirmation of topological thermal Hall effect in $CrXTe_3$ from thermal transport experiments.

In summary, we carried out a very comprehensive inelastic neutron scattering study of the spin-wave excitations on the ferromagnetic honeycomb magnets $CrXTe_3$. Our data show a clear gap opening in the magnon bands at the *K* points, with the gap size of about 2 and 5 meV for $CrSiTe_3$ and $CrGeTe_3$, respectively. The magnon band dispersion in $CrXTe_3$ can be described very well by either the Heisenberg-DM model or the Heisenberg-Kitaev model. The gap opening can be ascribed to the asymmetric DM interaction with an out-of-plane DM vector or Kitaev interactions. However, because of the very small magnetic anisotropy observed in $CrXTe_3$, the Heisenberg-DM model, in which the isotropic Heisenberg exchange dominates, is perceived as the proper model for these materials. The magnon spectra of $CrXTe_3$ are successfully reproduced by using the LSWT calculations. The gap size was found to be proportional to the strength of the DM interaction. The strength of the DM interaction is also strongly dependent on the SOC of the nonmagnetic Si/Ge atoms that are located at the honeycomb center. Furthermore, our numerical calculations predict the nontrivial topological nature of the magnon bands gap at the *K* points and also reveal the existence of topological edge states at the sample boundaries and domain walls. In addition, we also calculated the reference values for the expected thermal Hall conductivity that may arise from the topological magnon edge states, which can be measured in future thermal transport experiments. On the basis of our experimental and theoretical results, we propose that $CrSiTe_3$ and $CrGeTe_3$ present an ideal platform to realize topological magnon insulators, in which the nontrivial magnon gaps can be intrinsically tuned by varying the SOC of nonmagnetic ions. In contrast to CrI_3, the substitution of Si/Ge in the $CrXTe_3$ system using a wide range of nonmagnetic ions such as C, Si, Ge, Sn, Pb, and Ga (*46*–*50*) can, in principle, change the balance of the exchange interactions and, thus, enable the manipulation of the topological magnon gap size, leading to novel magnetic properties rooting in complex magnonic topology.

MATERIALS AND METHODS

High-quality single crystals of $CrXTe_3$ (X = Si, Ge) were grown by the flux method at the sample preparation laboratory of Jülich Centre for Neutron Science (JCNS) at Heinz Maier-Leibnitz Zentrum (MLZ) in Garching. Starting materials of Cr, X, and Te were mixed in an Ar-filled glove box at a molar ratio of Cr:X:Te = 1:1:10. The mixture was placed in an alumina crucible, which was then sealed in an evacuated quartz tube. The tube was heated up to 930°C (X = Ge) or 1030°C (X = Si) in 4 hours and sustained there for 10 hours. Then, the tube was slowly cooled down to 600°C with a cooling speed of 3°C/hour followed by separating the crystals from the Te flux by centrifuging. Shiny and sizable crystals with hexagonal natural edges were obtained.

Single-crystal x-ray diffraction was performed at room temperature with an incident wavelength of 1.54 Å (Cu-K_α) on a Bruker D2 PHASER x-ray diffractometer. By using a MPMS SQUID magnetometer (Quantum Design), the temperature and field dependence of the

magnetization of $CrSiTe_3$ and $CrGeTe_3$ were measured along both the *a* and *c* axes, respectively. The magnetic susceptibility was measured from 2 to 300 K with both zero-field-cooling and field-cooling conditions for some selected single crystals. The isothermal magnetization (*M*-*H*) curves were also measured in a sweeping field from −50 to 50 kOe at 2 K.

The polarized neutron diffraction measurement on single-crystal $CrGeTe_3$ was carried out at the cold-neutron polarized spectrometer DNS at MLZ (with $\lambda_i = 4.2$ Å) at $T = 4$ K. 2D Q maps in the (H,K,0) and (H,H,L) planes of reciprocal space at three different polarization modes were measured at 4 K. For the measurements of spin-wave excitations, we coaligned two pieces of large single crystals with a total mass of 1.3 g for $CrSiTe_3$ and more than 100 pieces with a total mass of about 1.4 g for $CrGeTe_3$. All the inelastic neutron scattering experiments were performed by using a range of thermal and cold neutron triple-axis spectrometers, including PUMA at MLZ, FLEXX (*51*) at HZB, and IN12, IN8, and IN22 at the Institut Laue-Langevin (ILL). Both the (H,H,L)- and (H,K,0)-oriented samples were prepared for each of $CrSiTe_3$ and $CrGeTe_3$. The low-energy magnon dispersion along [0,0,L] was measured at the cold neutron triple axis at IN12 (with a fixed $k_f = 1.7$ and 2.8 $Å^{-1}$) and at FLEXX (with $k_f = 1.55$ $Å^{-1}$). The magnon dispersions along [H,H,0] and [H,0,0] were measured at the thermal neutron triple-axis spectrometers IN8 and PUMA (both with a fixed $k_f = 2.662$ $Å^{-1}$). All the magnon dispersion data were collected at the base temperature of $T = 2$ K.

SUPPLEMENTARY MATERIALS

Supplementary material for this article is available at https://science.org/doi/10.1126/sciadv.abi7532

REFERENCES AND NOTES

1. F. D. M. Haldane, Model for a quantum Hall effect without Landau levels: Condensed-matter realization of the "parity anomaly". *Phys. Rev. Lett.* **61**, 2015–2018 (1988).
2. C. L. Kane, E. J. Mele, Z2 topological order and the quantum spin Hall effect. *Phys. Rev. Lett.* **95**, 146802 (2005).
3. M. Z. Hasan, C. L. Kane, Colloquium: Topological insulators. *Rev. Mod. Phys.* **82**, 3045–3067 (2010).
4. X.-L. Qi, S.-C. Zhang, Topological insulators and superconductors. *Rev. Mod. Phys.* **83**, 1057–1110 (2011).
5. N. P. Armitage, E. J. Mele, A. Vishwanath, Weyl and Dirac semimetals in three-dimensional solids. *Rev. Mod. Phys.* **90**, 015001 (2018).
6. N. Nagaosa, J. Sinova, S. Onoda, A. H. MacDonald, N. P. Ong, Anomalous Hall effect. *Rev. Mod. Phys.* **82**, 1539–1592 (2010).
7. D. Xiao, M.-C. Chang, Q. Niu, Berry phase effects on electronic properties. *Rev. Mod. Phys.* **82**, 1959–2007 (2010).
8. R. Chisnell, J. S. Helton, D. E. Freedman, D. K. Singh, R. I. Bewley, D. G. Nocera, Y. S. Lee, Topological magnon bands in a kagome lattice ferromagnet. *Phys. Rev. Lett.* **115**, 147201 (2015).
9. S. A. Owerre, A first theoretical realization of honeycomb topological magnon insulator. *J. Phys. Condens. Matter* **28**, 386001 (2016).
10. X. S. Wang, Y. Su, X. R. Wang, Topologically protected unidirectional edge spin waves and beam splitter. *Phys. Rev. B* **95**, 014435 (2017).
11. L. Chen, J.-H. Chung, B. Gao, T. Chen, M. B. Stone, A. I. Kolesnikov, Q. Huang, P. Dai, Topological spin excitations in honeycomb ferromagnet CrI_3. *Phys. Rev. X* **8**, 041028 (2018).
12. D. G. Joshi, Topological excitations in the ferromagnetic Kitaev-Heisenberg model. *Phys. Rev. B* **98**, 060405 (2018).
13. P. A. Pantaleón, Y. Xian, Edge states in a ferromagnetic honeycomb lattice with armchair boundaries. *Phys. B Condens. Matter* **530**, 191–194 (2018).
14. P. A. McClarty, X.-Y. Dong, M. Gohlke, J. G. Rau, F. Pollmann, R. Moessner, K. Penc, Topological magnons in Kitaev magnets at high fields. *Phys. Rev. B* **98**, 060404 (2018).
15. S. Bao, J. Wang, W. Wang, Z. Cai, S. Li, Z. Ma, D. Wang, K. Ran, Z.-Y. Dong, D. L. Abernathy, S.-L. Yu, X. Wan, J.-X. Li, J. Wen, Discovery of coexisting Dirac and triply degenerate magnons in a three-dimensional antiferromagnet. *Nat. Commun.* **9**, 2591 (2018).
16. W. Yao, C. Li, L. Wang, S. Xue, Y. Dan, K. Iida, K. Kamazawa, K. Li, C. Fang, Y. Li, Topological spin excitations in a three-dimensional antiferromagnet. *Nat. Phys.* **14**, 1011–1015 (2018).
17. B. Yuan, I. Khait, G.-J. Shu, F. C. Chou, M. B. Stone, J. P. Clancy, A. Paramekanti, Y.-J. Kim, Dirac magnons in a honeycomb lattice quantum *XY* magnet $CoTiO_3$. *Phys. Rev. X* **10**, 011062 (2020).
18. E. Aguilera, R. Jaeschke-Ubiergo, N. Vidal-Silva, L. E. F. Foa Torres, A. S. Nunez, Topological magnonics in the two-dimensional van der Waals magnet CrI_3. *Phys. Rev. B* **102**, 024409 (2020).
19. F. Mei, G. Chen, N. Goldman, L. Xiao, S. Jia, Topological magnon insulator and quantized pumps from strongly-interacting bosons in optical superlattices. *New J. Phys.* **21**, 095002 (2019).
20. A. Mook, J. Henk, I. Mertig, Magnon waveguide with nanoscale confinement constructed from topological magnon insulators. *Phys. Rev. B* **91**, 174409 (2015).
21. D. Malz, J. Knolle, A. Nunnenkamp, Topological magnon amplification. *Nat. Commun.* **10**, 3937 (2019).
22. L.-C. Zhang, D. Go, J.-P. Hanke, P. M. Buhl, S. Grytsiuk, S. Blügel, F. R. Lux, Y. Mokrousov, Imprinting and driving electronic orbital magnetism using magnons. *Commun. Phys.* **3**, 227 (2020).
23. H. Katsura, N. Nagaosa, P. A. Lee, Theory of the thermal Hall effect in quantum magnets. *Phys. Rev. Lett.* **104**, 066403 (2010).
24. Y. Onose, T. Ideue, H. Katsura, Y. Shiomi, N. Nagaosa, Y. Tokura, Observation of the magnon Hall effect. *Science* **329**, 297–299 (2010).
25. R. Matsumoto, S. Murakami, Theoretical prediction of a rotating magnon wave packet in ferromagnets. *Phys. Rev. Lett.* **106**, 197202 (2011).
26. S. A. Owerre, Topological honeycomb magnon Hall effect: A calculation of thermal Hall conductivity of magnetic spin excitations. *J. Appl. Phys.* **120**, 043903 (2016).
27. C. Gong, L. Li, Z. Li, H. Ji, A. Stern, Y. Xia, T. Cao, W. Bao, C. Wang, Y. Wang, Z. Q. Qiu, R. J. Cava, S. G. Louie, J. Xia, X. Zhang, Discovery of intrinsic ferromagnetism in two-dimensional van der Waals crystals. *Nature* **546**, 265–269 (2017).
28. B. Ding, Z. Li, G. Xu, H. Li, Z. Hou, E. Liu, X. Xi, F. Xu, Y. Yao, W. Wang, Observation of magnetic skyrmion bubbles in a van der Waals Ferromagnet Fe_3GeTe_2. *Nano Lett.* **20**, 868–873 (2020).
29. Y. Kasahara, T. Ohnishi, Y. Mizukami, O. Tanaka, S. Ma, K. Sugii, N. Kurita, H. Tanaka, J. Nasu, Y. Motome, T. Shibauchi, Y. Matsuda, Majorana quantization and half-integer thermal quantum Hall effect in a Kitaev spin liquid. *Nature* **559**, 227–231 (2018).
30. T. Moriya, New mechanism of anisotropic superexchange interaction. *Phys. Rev. Lett.* **4**, 228–230 (1960).
31. M. A. McGuire, H. Dixit, V. R. Cooper, B. C. Sales, Coupling of crystal structure and magnetism in the layered, ferromagnetic insulator CrI_3. *Chem. Mater.* **27**, 612–620 (2015).
32. L. D. Casto, A. J. Clune, M. O. Yokosuk, J. L. Musfeldt, T. J. Williams, H. L. Zhuang, M.-W. Lin, K. Xiao, R. G. Hennig, B. C. Sales, J.-Q. Yan, D. Mandrus, Strong spin-lattice coupling in $CrSiTe_3$. *APL Mater.* **3**, 041515 (2015).
33. B. Liu, Y. Zou, L. Zhang, S. Zhou, Z. Wang, W. Wang, Z. Qu, Y. Zhang, Critical behavior of the quasi-two-dimensional semiconducting ferromagnet $CrSiTe_3$. *Sci. Rep.* **6**, 33873 (2016).
34. D.-H. Kim, K. Kim, K.-T. Ko, J. Seo, J. S. Kim, T.-H. Jang, Y. Kim, J.-Y. Kim, S.-W. Cheong, J.-H. Park, Giant magnetic anisotropy induced by ligand LS coupling in layered Cr compounds. *Phys. Rev. Lett.* **122**, 207201 (2019).
35. J. Zeisner, A. Alfonsov, S. Selter, S. Aswartham, M. P. Ghimire, M. Richter, J. van den Brink, B. Büchner, V. Kataev, Magnetic anisotropy and spin-polarized two-dimensional electron gas in the van der Waals ferromagnet $Cr_2Ge_2Te_6$. *Phys. Rev. B* **99**, 165109 (2019).
36. K. Wang, T. Hu, F. Jia, G. Zhao, Y. Liu, I. V. Solovyev, A. P. Pyatakov, A. K. Zvezdin, W. Ren, Magnetic and electronic properties of $Cr_2Ge_2Te_6$ monolayer by strain and electric-field engineering. *Appl. Phys. Lett.* **114**, 092405 (2019).
37. Y. Tian, M. J. Gray, H. Ji, R. J. Cava, K. S. Burch, Magneto-elastic coupling in a potential ferromagnetic 2D atomic crystal. *2D Mater.* **3**, 025035 (2016).
38. Y. Sun, R. C. Xiao, G. T. Lin, R. R. Zhang, L. S. Ling, Z. W. Ma, X. Luo, W. J. Lu, Y. P. Sun, Z. G. Sheng, Effects of hydrostatic pressure on spin-lattice coupling in two-dimensional ferromagnetic $Cr_2Ge_2Te_6$. *Appl. Phys. Lett.* **112**, 072409 (2018).
39. K. Wang, X. Xu, Y. Cheng, M. Zhang, J. S. Wang, H. Wang, G. Zhang, Magnon relaxation time in ferromagnetic $Cr_2Ge_2Te_6$ monolayer governed by magnon-phonon interaction. *Appl. Phys. Lett.* **118**, 023102 (2021).
40. F. J. dos Santos, M. dos Santos Dias, F. S. M. Guimarães, J. Bouaziz, S. Lounis, Spin-resolved inelastic electron scattering by spin waves in noncollinear magnets. *Phys. Rev. B* **97**, 024431 (2018).
41. J. B. Goodenough, *Magnetism and the Chemical Bond* (Interscience-Wiley, 1963).
42. S. K. Kim, H. Ochoa, R. Zarzuela, Y. Tserkovnyak, Realization of the Haldane-Kane-Mele model in a system of localized spins. *Phys. Rev. Lett.* **117**, 227201 (2016).
43. A. Banerjee, C. A. Bridges, J.-Q. Yan, A. A. Aczel, L. Li, M. B. Stone, G. E. Granroth, M. D. Lumsden, Y. Yiu, J. Knolle, S. Bhattacharjee, D. L. Kovrizhin, R. Moessner, D. A. Tennant, D. G. Mandrus, S. E. Nagler, Proximate Kitaev quantum spin liquid behaviour in a honeycomb magnet. *Nat. Mater.* **15**, 733–740 (2016).

44. M. Zhu, D. Do, C. R. Dela Cruz, Z. Dun, H. D. Zhou, S. D. Mahanti, X. Ke, Tuning the magnetic exchange via a control of orbital hybridization in $Cr_2(Te_{1-x}W_x)O_6$. *Phys. Rev. Lett.* **113**, 076406 (2014).
45. V. M. Katukuri, P. Babkevich, O. Mustonen, H. C. Walker, B. Fåk, S. Vasala, M. Karppinen, H. M. Rønnow, O. V. Yazyev, Exchange interactions mediated by nonmagnetic cations in double perovskites. *Phys. Rev. Lett.* **124**, 077202 (2020).
46. S. Chabungbam, P. Sen, Computational design of a robust two-dimensional antiferromagnetic semiconductor. *Phys. Rev. B* **96**, 045404 (2017).
47. H. L. Zhuang, Y. Xie, P. R. C. Kent, P. Ganesh, Computational discovery of ferromagnetic semiconducting single-layer $CrSnTe_3$. *Phys. Rev. B* **92**, 035407 (2015).
48. I. Khan, J. Hong, High Curie temperature and strain-induced semiconductor-metal transition with spin reorientation transition in 2D $CrPbTe_3$ monolayer. *Nanotechnology* **31**, 195704 (2020).
49. B. Marfoua, J. Hong, Spin Seebeck effect in the 2D ferromagnetic $CrPbTe_3$. *Phys. E Low Dimens. Syst. Nanostructures* **126**, 114443 (2021).
50. M. Yu, X. Liu, W. Guo, Novel two-dimensional ferromagnetic semiconductors: Ga-based transition-metal trichalcogenide monolayers. *Phys. Chem. Chem. Phys.* **20**, 6374–6382 (2018).
51. M. D. Le, D. L. Quintero-Castro, R. Toft-Petersen, F. Groitl, M. Skoulatos, K. C. Rule, K. Habicht, Gains from the upgrade of the cold neutron triple-axis spectrometer FLEXX at the BER-II reactor. *Nucl. Instrum. Methods Phys. Res. A* **729**, 220–226 (2013).
52. V. Carteaux, D. Brunet, G. Ouvrard, G. Andre, Crystallographic, magnetic and electronic structures of a new layered ferromagnetic compound $Cr_2Ge_2Te_6$. *J. Phys. Condens. Matter* **7**, 69 (1995).
53. Y. F. Li, W. Wang, W. Guo, C. Y. Gu, H. Y. Sun, L. He, J. Zhou, Z. B. Gu, Y. F. Nie, X. Q. Pan, Electronic structure of ferromagnetic semiconductor $CrGeTe_3$ by angle-resolved photoemission spectroscopy. *Phys. Rev. B* **98**, 125127 (2018).
54. S. Khan, C. W. Zollitsch, D. M. Arroo, H. Cheng, I. Verzhbitskiy, A. Sud, Y. P. Feng, G. Eda, H. Kurebayashi, Spin dynamics study in layered van der Waals single-crystal $Cr_2Ge_2Te_6$. *Phys. Rev. B* **100**, 134437 (2019).
55. T. Holstein, H. Primakoff, Field dependence of the intrinsic domain magnetization of a ferromagnet. *Phys. Rev.* **58**, 1098–1113 (1940).
56. Y. Singh, S. Manni, J. Reuther, T. Berlijn, R. Thomale, W. Ku, S. Trebst, P. Gegenwart, Relevance of the Heisenberg-Kitaev model for the honeycomb lattice iridates A_2IrO_3. *Phys. Rev. Lett.* **108**, 127203 (2012).
57. C. Xu, J. Feng, H. Xiang, L. Bellaiche, Interplay between Kitaev interaction and single ion anisotropy in ferromagnetic CrI_3 and $CrGeTe_3$ monolayers. *npj Comput. Mater.* **4**, 57 (2018).
58. L.-C. Zhang, F. Zhu, D. Go, F. R. Lux, F. J. dos Santos, S. Lounis, Y. Su, S. Blügel, Y. Mokrousov, Interplay of Dzyaloshinskii-Moriya and Kitaev interactions for magnonic properties of Heisenberg-Kitaev honeycomb ferromagnets. *Phys. Rev. B* **103**, 134414 (2021).
59. C. Xu, J. Feng, M. Kawamura, Y. Yamaji, Y. Nahas, S. Prokhorenko, Y. Qi, H. Xiang, L. Bellaiche, Possible Kitaev quantum spin liquid state in 2D materials with $S = 3/2$. *Phys. Rev. Lett.* **124**, 087205 (2020).
60. A. Mook, J. Henk, I. Mertig, Magnon Hall effect and topology in kagome lattices: A theoretical investigation. *Phys. Rev. B* **89**, 134409 (2014).

Acknowledgments: We acknowledge S. Mayr for assistance with the crystal orientation. This work is based on the experiments performed at DNS, PUMA, IN8, IN12, IN22, and FLEXX neutron instruments. **Funding:** F.Z. acknowledges the funding support from the HGF-OCPC Postdoctoral Program. Y.M. acknowledges the Jülich Supercomputing Centre and RWTH Aachen University for providing computational resources, as well as the support of Deutsche Forschungsgemeinschaft (DFG, German Research Foundation)—TRR 173 268565370 (project A11) and TRR 288 422213477 (project B06). L.Z. acknowledges the support of China Scholarship Council (CSC) (grant no. [2016]3100). S.L. acknowledges the funding support provided by the Priority Programme SPP 2244 2D Materials Physics of van der Waals Heterostructures of the Deutsche Forschungsgemeinschaft (DFG) (project LO 1659/7-1) and the European Research Council (ERC) under the European Union's Horizon 2020 research and innovation programme (ERC-consolidator grant no. 681405 DYNASORE). S.B. acknowledges financial support from the Deutsche Forschungsgemeinschaft (DFG) within CRC 1238 (project number 277146847, subproject C01). J.M. acknowledges the financial support from the National Science Foundation of China (no. 11774223 and no. U2032213). **Author contributions:** F.Z. and Y.S. conceived the project. Y.S., Y.M., S.B., and T.B. co-supervised the work. X.W. carried out the single-crystal growth. F.Z., X.W., and Y.S. carried out the neutron scattering experiments with support from J.S., T.M., K.S., W.F.S., A.I., J.T.P., J.X., and J.M. L.Z. carried out the theoretical analysis with support from F.J.d.S., S.L., and Y.M. F.Z. carried out the x-ray diffraction and magnetization measurements. F.Z., L.Z., and Y.S. wrote the manuscript with contributions from all authors. **Competing interests:** The authors declare that they have no competing interests. **Data and materials availability:** All data needed to evaluate the conclusions in the paper are present in the paper and/or the Supplementary Materials. The raw data taken at the Institut Laue-Langevin (ILL) can be accessed at https://doi.ill.fr/10.5291/ILL-DATA.4-01-1634 and https://doi.ill.fr/10.5291/ILL-DATA.CRG-2498. The raw data taken at the Heinz Maier-Leibnitz Zentrum (MLZ) and at the Berlin Neutron Scattering Center (BENSC) can be accessed at https://doi.org/10.5281/zenodo.4963138.

Submitted 29 March 2021
Accepted 21 July 2021
Published 10 September 2021
10.1126/sciadv.abi7532

Citation: F. Zhu, L. Zhang, X. Wang, F. J. dos Santos, J. Song, T. Mueller, K. Schmalzl, W. F. Schmidt, A. Ivanov, J. T. Park, J. Xu, J. Ma, S. Lounis, S. Blügel, Y. Mokrousov, Y. Su, T. Brückel, Topological magnon insulators in two-dimensional van der Waals ferromagnets $CrSiTe_3$ and $CrGeTe_3$: Toward intrinsic gap-tunability. *Sci. Adv.* **7**, eabi7532 (2021).

ScienceAdvances

Topological magnon insulators in two-dimensional van der Waals ferromagnets CrSiTe and CrGeTe: Toward intrinsic gap-tunability

Fengfeng ZhuLichuan ZhangXiao WangFlaviano José dos SantosJunda SongThomas MuellerKarin SchmalzlWolfgang F. SchmidtAlexandre IvanovJitae T. ParkJianhui XuJie MaSamir LounisStefan BlügelYuriy MokrousovYixi SuThomas Brückel

Sci. Adv., 7 (37), eabi7532. • DOI: 10.1126/sciadv.abi7532

Science Advances (ISSN) is published by the American Association for the Advancement of Science. 1200 New York Avenue NW, Washington, DC 20005. The title *Science Advances* is a registered trademark of AAAS.